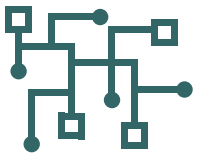

ISE

Industrial and Systems Engineering

Large-Scale Discrete Multi-Scenario Truss Sizing Optimization: Model Analysis and Computational Methodology Experiments

RAMIN FAKHIMI[1], MOHAMMAD SHAHABSAFA[1], WEIMING LEI[1], TAMÁS TERLAKY[1], LUIS F. ZULUAGA[1], SICHENG HE[2], JOHN T. HWANG[2], AND JOAQUIM R. R. A. MARTINS[2]

[1]Department of Industrial and Systems Engineering, Lehigh University, Bethlehem, PA, USA

[2]Dept. of Aerospace Engineering University of Michigan, Ann Arbor, MI, USA

ISE Technical Report 20T-022

LEHIGH UNIVERSITY

Large-Scale Discrete Multi-Scenario Truss Sizing Optimization: Model Analysis and Computational Methodology Experiments

Ramin Fakhimi[1], Mohammad Shahabsafa[1], Weiming Lei[1], Tamás Terlaky[1], Luis F. Zuluaga[1], Sicheng He[2], John T. Hwang[2], and Joaquim R. R. A. Martins[2]

[1]Department of Industrial and Systems Engineering, Lehigh University, Bethlehem, PA, USA

[2]Dept. of Aerospace Engineering University of Michigan, Ann Arbor, MI, USA

October 2, 2020

Abstract

Discrete multi-scenario truss sizing optimization problems (MSTSO) are challenging to solve due to their combinatorial, nonlinear, and non-convex nature. In this study, we highlight two important characteristics of the feasible set of MSTSO problems. First, given a feasible truss structure for the continuous MSTSO problem, we show that an appropriate scaling of the cross-sectional areas preserves the feasibility of the new structure. Second, we prove that a truss structure that withstands a set of external force scenarios also withstands any scenario that lies in the convex hull of those external force scenarios. Taking advantage of these characteristics, we extend the neighborhood search mixed integer linear optimization (NS-MILO) method Shahabsafa et al. (2018) to solve discrete MSTSO problems. Through extensive computational experiments, we demonstrate that the NS-MILO method provides high-quality solutions for large-scale discrete MSTSO problems in a reasonable time.

1 Introduction

Truss structures are widely used in a variety of infrastructures like bridges and buildings. A truss design problem is concerned with the optimal design of a truss structure with respect to an objective, e.g., the weight of the structure, while considering several mechanical constraints. In a truss design problem, the shape and the topology of the structure, as well as the cross-sectional areas of bars can be considered (Topping, 1983; Ben-Tal and Bendsøe, 1993). In truss sizing optimization (TSO) problems, the truss topology is given and the cross sectional areas of bars are to be decided (Dorn et al., 1964). In real world applications, a truss structure should withstand different loading conditions. We refer to these problems as *multi-scenario truss sizing optimization (MSTSO)* problems. A variety of models assume that that the cross-sectional areas of the bars can be selected from a continuous range (Stolpe, 2004; Degertekin, 2012); while others consider a more realistic situation in which the cross-sectional areas of the bars are required to belong to a discrete set of options (Achtziger, 1998; Achtziger and Stolpe, 2007a,b,c; Mela, 2014).

Mellaert et al. (2016) proposed a mixed integer linear optimization (MILO) model for discrete single scenario TSO problems considering displacement constraints, member constraints, and joint constraints. Shahabsafa et al. (2018) proposed a MILO model for discrete single scenario TSO problems with weight as its objective function. They considered additional physical constraints such as Hooke's law and Euler buckling constraints. In truss topology design (TTD) problems, potential bars can take zero cross-sectional areas. Achtziger (1998) studied the discrete truss topology design and sizing optimization problem with

the objective of minimizing the maximum compliance considering multiple external force scenarios. Mela (2014) suggested a MILO model for discrete multi-scenario truss topology design and sizing optimization problems considering physical constraints.

There is another class of problems which can be reformulated as a MSTSO problem; namely, when the structure is under uncertain load scenarios (Lógó et al., 2009). Stochastic optimization is a mathematical approach to deal with uncertainty by considering random variables in the problem. In special cases, for example, when one has discrete random variables, a stochastic problem can be reformulated as a multi-scenario problem (Csébfalvi, 2018). Alvarez and Carrasco (2005) demonstrated that the minimum expected compliance under stochastic load scenarios coincides with the dual of a special convex minimax problem. They proved that the expected compliance minimization problem is equivalent to a multiload problem with a specific finite set of multiple load scenarios. Makrodimopoulos et al. (2010) proposed a new compliance-based objective for the truss design problem under multiple load scenarios. Their model minimizes the summation of the maximum strain energy of the structure. They proved that in kinematically stable and determinate structures the proposed problem is equivalent to a weight minimization problem.

It should be noted that uncertainty in force scenarios can also be modeled using robust optimization instead of stochastic optimization (Calafiore and Dabbene, 2008; Zhao and Wang, 2014). In these cases, the problem typically cannot be reformulated as a MSTSO problem. Kanno and Takewaki (2006) applied the quadratic embedding method of uncertainty and the S-procedure (Ben-Tal and Nemirovski, 2001) and reformulated the problem as a nonlinear semidefinite optimization problem. Dunning et al. (2011) considered uncertainties in the external loads' magnitude and direction in the compliance minimization problem. They applied an analytical approach for normally distributed external forces and converted the robust optimization problem into a multiple load scenarios problem. Liu and Gea (2018) proposed a new continuous formulation for TTDSO problems where bars are under uncertain forces. The ellipsoid-bounded uncertainty comes from both the external loads' magnitude and direction. The objective is to minimize the maximum compliance.

Several authors tried to tackle truss design problems under multiple external force scenarios (see e.g., Lamberti, 2008; Azad and Hasançebi, 2015; Do and Lee, 2017). Smith (1997) extended the heuristic method that is developed by Pedersen (1993) for single-scenario truss design problems to solve multi-scenario topology design and sizing optimization problems. Cheng et al. (2016a) and Lee et al. (2005) proposed a harmony search algorithm to solve discrete MSTSO problems. They considered some bounds constraints for yield stress, nodal displacement, and Euler buckling constraints. However, they did not formally show how to relate yield stress and nodal displacement to the cross-sectional areas of the bars. Azad and Hasançebi (2014a) developed a neighborhood search meta-heuristic algorithm for discrete MSTSO problems without considering Euler buckling constraints. Capriles et al. (2007) and Camp and Farshchin (2014) suggested an ant colony algorithm for the discrete MSTSO problems without considering the effect of Euler buckling constraint on the problem. To enforce the physical constraints they used a penalty function. Stolpe (2016) comprehensively reviewed the methods that were used to solve truss design problems.

Our goal in this paper is to solve large-scale MSTSO problems. We consider the minimum-weight MSTSO problem with force balance equations, Hooke's law, yield stress bounds, displacement bounds, and Euler buckling constraints (Shahabsafa et al., 2018). We present two important characteristics of the feasible set of MSTSO problems: (a). Given a feasible truss structure for the continuous MSTSO problem, we prove that a proportional scaling of cross-sectional areas, up to their upper bounds, remains feasible for the problem. (b). We also prove that adding any convex combination of existing external force scenarios does not change the feasible set of the MSTSO problem. As the size of the truss structures grow, it becomes increasingly difficult to find a proven optimal solution for discrete MSTSO problems. To overcome this difficulty, we extend the neighborhood search mixed integer linear optimization (NS-MILO) method (Shahabsafa et al., 2018), that performs well in providing high-quality solutions for single-scenario discrete TSO problems, to solve MSTSO problems. By solving various classical and large-scale test problems, we demonstrate that the extended NS-MILO method provides high-quality solutions for MSTSO problems.

The rest of the article is organized as follows. In Section 2, we formally introduce both the continuous and discrete MSTSO problems. In Section 3, we present two important properties of the feasible set of MSTSO problems. In Section 4, we present the extension of the NS-MILO method for MSTSO problems. Then, through extensive computational experiments, we demonstrate the efficiency of the extended NS-MILO method in solving large-scale MSTSO problems.

2 Problem description

In this article, we consider multi-scenario TSO problems. Our mathematical optimization model for MSTSO problems is a reformulation of the TSO model introduced by Shahabsafa et al. (2018).

We discuss different dimensions of the problem. Let m and n denote the number of bars and degrees of freedom of the ground structure, respectively. The dimension of the space is denoted by d ($d = 2, 3$). We assume that each node is either fixed in all directions or pinned. Let $\mathcal{I} = \{1, \ldots, m\}$ be the index set of the bars of the ground structure and let $\mathcal{H} = \{1, \ldots, p\}$ represent the index set of the external force scenarios, where p denotes the number of the external force scenarios.

Vector $x \in \mathbb{R}^m_{++}$ denotes the cross-sectional areas of the bars, where $\mathbb{R}^m_{++}$ is the m-dimensional space of strictly positive vectors. Let $f^h \in \mathbb{R}^n$, for $h \in \mathcal{H}$, denote the vector of the external forces in scenario h. Let $q^h \in \mathbb{R}^m$, for $h \in \mathcal{H}$, represent the vector of the internal forces of scenario h. The relationship between the external forces and internal forces are governed by the following force balance equations:

$$Rq^h = f^h, \quad h \in \mathcal{H},$$

where $R \in \mathbb{R}^{n \times m}$ is the topology matrix of the truss structure.

The stress on bar $i \in \mathcal{I}$ in scenario $h \in \mathcal{H}$ is denoted by σ_i^h, and is defined as

$$\sigma_i^h = \frac{q_i^h}{x_i}.$$

Let $u^h \in \mathbb{R}^n$ and $\Delta l^h \in \mathbb{R}^m$, for $h \in \mathcal{H}$, denote the nodal displacements and the elongations of the bars in scenario h, respectively. The relationship between the nodal displacements and the elongations of the bars is as follows:

$$\Delta l^h = R^T u^h, \quad h \in \mathcal{H}. \tag{1}$$

Let E_i and l_i, for $i \in \mathcal{I}$, be the Young's modulus and the length of bar $i \in \mathcal{I}$, respectively. Hooke's law governs the relationship between the stress and elongation of the bars; namely

$$\sigma_i^h = \frac{E_i}{l_i} \Delta l_i^h, \quad i \in \mathcal{I}, h \in \mathcal{H}. \tag{2}$$

The cross-sectional areas of the bars are assumed to be circular. Let $\gamma_i = \pi E_i / 4 l_i^2$ for $i \in \mathcal{I}$. The Euler buckling constraints are written as

$$\sigma_i^h + \gamma_i x_i \geq 0, \quad i \in \mathcal{I}, h \in \mathcal{H}. \tag{3}$$

Let $\sigma^{\min}, \sigma^{\max} \in \mathbb{R}^m$ be the lower and upper bounds on the stress of the bars where $\sigma^{\min} < 0 < \sigma^{\max}$. Let $x^{\min}, x^{\max} \in \mathbb{R}^m$ be the lower and upper bounds on the bars' cross-sectional areas. Also, let $u^{\min}, u^{\max} \in \mathbb{R}^n$ denote the lower and upper bounds of the nodal displacements, respectively. We set $u^{\min} < 0 < u^{\max}$ to make it general.

Let ρ be the density of the material used to construct the truss structure. The objective is to minimize the total weight of the structure, which is equal to $\rho\, l^T x$. The continuous MSTSO problem can be formulated as follows:

$$
\begin{array}{lllllll}
\min & \rho\, l^T x, & & & & & \\
\text{s.t.} & Rq^h & = & f^h, & & h \in \mathcal{H}, \\
& R^T u^h & = & \Delta l^h, & & h \in \mathcal{H}, \\
& \frac{E_i}{l_i}\Delta l_i^h - \sigma_i^h & = & 0, & & i \in \mathcal{I}, h \in \mathcal{H}, \\
& q_i^h - x_i \sigma_i^h & = & 0, & & i \in \mathcal{I}, h \in \mathcal{H}, \\
& \sigma_i^h + \gamma_i x_i & \geq & 0, & & i \in \mathcal{I}, h \in \mathcal{H}, \\
& u^{\min} & \leq & u^h & \leq u^{\max}, & h \in \mathcal{H}, \\
& \sigma^{\min} & \leq & \sigma^h & \leq \sigma^{\max}, & h \in \mathcal{H}, \\
& x^{\min} & \leq & x & \leq x^{\max}. &
\end{array}
\tag{4}
$$

In model (4), the cross-sectional areas of the bars are assumed to be continuous decision variables. However, in practice, due to manufacturing and economic restrictions, bars frequently take values only from a predefined discrete set (Achtziger and Stolpe, 2007a). Without loss of generality, we may assume that the number of candidate sizes is the same for all the bars. Furthermore, for ease of presentation, we assume that all the bars have the same set $\mathcal{S}$ of potential cross-sectional areas. Let $\mathcal{S}$ be the set of possible non-zero cross-sectional areas of the bars defined as:

$$
\mathcal{S} = \{s_1, s_2, \ldots, s_v\}, \tag{5}
$$

where $0 < s_1 \leq s_2 \leq \ldots \leq s_v$ and v is the cardinality of the set $\mathcal{S}$. Let $\mathcal{K} = \{1, \ldots, v\}$ denote the set of indices corresponding to the discrete set $\mathcal{S}$. The cross-sectional area of bar i, for $i \in \mathcal{I}$, takes values from the set $\mathcal{S}$ in the discrete MSTSO problem. Next, we apply the *incremental* model proposed by Shahabsafa et al. (2018, Section 2.2) for the discrete single-scenario TSO problems, to discrete MSTSO problem. Let $\bar{\mathcal{K}} = \{1, \ldots, v-1\}$ and $\delta_k = s_{k+1} - s_k$ for $k \in \bar{\mathcal{K}}$. The incremental formulation of choosing from the discrete set of cross-sectional areas is as follows:

$$
\begin{array}{ll}
x_i = \displaystyle\sum_{k \in \bar{\mathcal{K}}} \delta_k z_{ik}, & i \in \mathcal{I}, \\
z_{ik} \leq z_{i,k-1}, & i \in \mathcal{I},\ k \in \bar{\mathcal{K}} \setminus \{1\}, \\
z_{ik} \in \{0, 1\}, & i \in \mathcal{I},\ k \in \bar{\mathcal{K}}.
\end{array}
\tag{6}
$$

Let σ_{ik}^h, for $i \in \mathcal{I}$, $k \in \mathcal{K}$ and $h \in \mathcal{H}$, be the stress on bar i in scenario h if $x_i = s_k$, that is

$$
\sigma_{ik}^h = \begin{cases} \frac{E_i}{l_i}\Delta l_i^h, & \text{if } x_i = s_k; \\ 0, & \text{otherwise.} \end{cases}
$$

Notice that $\sigma_i^h = \sum_{k \in \mathcal{K}} \sigma_{ik}^h$. The following set of constraints enforce yield stress and Euler buckling constraints:

$$
\begin{array}{lll}
\max\left(-\gamma_i s_1, \sigma_i^{\min}\right)(1 - z_{i1}) \leq \sigma_{i1}^h \leq \sigma_i^{\max}(1 - z_{i1}), & i \in \mathcal{I}, h \in \mathcal{H}, \\
\max\left(-\gamma_i s_k, \sigma_i^{\min}\right)(z_{i,k-1} - z_{ik}) \leq \sigma_{ik}^h \leq \sigma_i^{\max}(z_{i,k-1} - z_{ik}), & i \in \mathcal{I}, k \in \bar{\mathcal{K}} \setminus \{1\}, h \in \mathcal{H}, \\
\max\left(-\gamma_i s_v, \sigma_i^{\min}\right) z_{i,v-1} \leq \sigma_{iv}^h \leq \sigma_i^{\max} z_{i,v-1}, & i \in \mathcal{I}, h \in \mathcal{H}.
\end{array}
$$

The discrete MSTSO problem can then be formulated as:

$$
\begin{array}{lllll}
\min & \rho\, l^T x, & & & \\
\text{s.t.} & Rq^h & = f^h, & & h \in \mathcal{H}, \\
& R^T u^h & = \Delta l^h, & & h \in \mathcal{H}, \\
& x_i - s_1 - \sum_{k \in \bar{\mathcal{K}}} \delta_k z_{ik} & = 0, & & i \in \mathcal{I}, \\
& \frac{E_i}{l_i} \Delta l_i^h - \sum_{k \in \mathcal{K}} \sigma_{ik}^h & = 0, & & i \in \mathcal{I}, h \in \mathcal{H}, \\
& q_i^h - \sum_{k \in \mathcal{K}} s_k \sigma_{ik}^h & = 0, & & i \in \mathcal{I}, h \in \mathcal{H}, \\
& z_{ik} & \leq z_{i,k-1}, & & i \in \mathcal{I},\ k \in \bar{\mathcal{K}} \setminus \{1\}, \\
& u^{\min} & \leq u^h & \leq u^{\max}, & h \in \mathcal{H}, \\
& \max\left(-\gamma_i s_1, \sigma_i^{\min}\right)(1 - z_{i1}) & \leq \sigma_{i1}^h & \leq \sigma_i^{\max}(1 - z_{i1}), & i \in \mathcal{I}, h \in \mathcal{H}, \\
& \max\left(-\gamma_i s_k, \sigma_i^{\min}\right)(z_{i,k-1} - z_{ik}) & \leq \sigma_{ik}^h & \leq \sigma_i^{\max}(z_{i,k-1} - z_{ik}), & i \in \mathcal{I}, k \in \bar{\mathcal{K}} \setminus \{1\}, h \in \mathcal{H}, \\
& \max\left(-\gamma_i s_v, \sigma_i^{\min}\right) z_{i,v-1} & \leq \sigma_{iv}^h & \leq \sigma_i^{\max} z_{i,v-1}, & i \in \mathcal{I}, h \in \mathcal{H}, \\
& z_{ik} \in \{0,1\}, & & & i \in \mathcal{I},\ k \in \bar{\mathcal{K}}.
\end{array}
\tag{7}
$$

In Section 3, we present two important characteristics of the feasible set of the continuous MSTSO problem (4), one of which holds for the discrete MSTSO problem (7) as well.

3 Theoretical properties of MSTSO problems

In this section, we present two important properties of the feasible set of the MSTSO problem (4). These properties are then used in extending the NS-MILO method (Shahabsafa et al., 2018) to solve large-scale discrete MSTSO problems.

Let $\mathcal{F}$ be the feasible set of the continuous MSTSO problem (4) and let $(x, u, \Delta l, \sigma, q) \in \mathcal{F}$ be a feasible solution for problem (4), where

$$
\begin{array}{lll}
u \coloneqq (u^1, \ldots, u^p), & u^h \in \mathbb{R}^n, & h \in \mathcal{H}, \\
\Delta l \coloneqq (\Delta l^1, \ldots, \Delta l^p), & \Delta l^h \in \mathbb{R}^m, & h \in \mathcal{H}, \\
\sigma \coloneqq (\sigma^1, \ldots, \sigma^p), & \sigma^h \in \mathbb{R}^m, & h \in \mathcal{H}, \\
q \coloneqq (q^1, \ldots, q^p), & q^h \in \mathbb{R}^m, & h \in \mathcal{H}.
\end{array}
\tag{8}
$$

Let $\mathcal{X}$ denote the m-dimensional subspace of the bars' cross-sectional areas. Additionally, let $\mathcal{F}_{\mathcal{X}}$ denote the orthogonal projection of the feasible set $\mathcal{F}$ on the subspace $\mathcal{X}$, that is, $\mathcal{F}_{\mathcal{X}} = \{x \in \mathbb{R}^m_{++} : \exists\,(u, \Delta l, \sigma, q) \text{ s.t. } (x, u, \Delta l, \sigma, q) \in \mathcal{F}\}$. In what follows, the truss structure corresponding to cross-sectional area $x \in \mathbb{R}^m$ is referred to as *structure* x.

3.1 Feasibility along rays

In this section, we prove that any scaling of a feasible structure x for the continuous MSTSO problem (4) with coefficient $\alpha \geq 1$ is also feasible for problem (4), if αx satisfies the upper bounds of the cross-sectional areas; that is, $\alpha x \leq x^{\max}$.

Theorem 3.1. *Let $x \in \mathcal{F}_{\mathcal{X}}$ and $\alpha \geq 1$. If $\alpha x \leq x^{\max}$, then $\alpha x \in \mathcal{F}_{\mathcal{X}}$.*

Proof. As $x \in \mathcal{F}_{\mathcal{X}}$, there exists $(u, \Delta l, \sigma, q)$ such that $(x, u, \Delta l, \sigma, q) \in \mathcal{F}$, (see (8)). Let $\bar{x} = \alpha x$, and let $(\bar{u}, \overline{\Delta l}, \bar{\sigma}, \bar{q})$ be defined as follows:

$$\begin{aligned} \bar{u}^h &= \frac{1}{\alpha}\, u^h, \qquad \forall h \in \mathcal{H}, \\ \overline{\Delta l}^h &= \frac{1}{\alpha}\, \Delta l^h, \quad \forall h \in \mathcal{H}, \\ \bar{\sigma}^h &= \frac{1}{\alpha}\, \sigma^h, \qquad \forall h \in \mathcal{H}, \\ \bar{q}^h &= q^h, \qquad \forall h \in \mathcal{H}. \end{aligned} \tag{9}$$

From (1), (2) and (9), we have

$$\begin{aligned} \overline{\Delta l}^h &= \frac{1}{\alpha} R^T u^h = R^T \bar{u}^h, \qquad h \in \mathcal{H}, \\ \bar{\sigma}_i^h &= \frac{1}{\alpha}\frac{E_i}{l_i}\Delta {l_i}^h = \frac{E_i}{l_i}\overline{\Delta l}_i^h, \quad i \in \mathcal{I}, h \in \mathcal{H}. \end{aligned}$$

If $\sigma_i^h \geq 0$ for $i \in \mathcal{I}, h \in \mathcal{H}$, then we have $\bar{\sigma}_i^h + \gamma_i \bar{x}_i \geq 0$. Now, if $\sigma_i^h < 0$, for $i \in \mathcal{I}$ and $h \in \mathcal{H}$, then we have

$$\bar{\sigma}_i^h + \gamma_i \bar{x}_i = \frac{1}{\alpha}\sigma_i^h + \gamma_i \alpha x_i \geq \sigma_i^h + \gamma_i x_i \geq 0.$$

If $\sigma_i^h \geq 0$, for $i \in \mathcal{I}$ and $h \in \mathcal{H}$, then

$$\sigma^{\min} \leq 0 \leq \frac{\sigma_i^h}{\alpha} = \bar{\sigma}_i^h \leq \sigma_i^h \leq \sigma^{\max}.$$

Also, if $\sigma_i^h < 0$, for $i \in \mathcal{I}$ and $h \in \mathcal{H}$, then

$$\sigma_i^{\min} \leq \sigma_i^h \leq \frac{\sigma_i^h}{\alpha} = \bar{\sigma}_i^h \leq 0 \leq \sigma_i^{\max}.$$

Similarly, one can show that $u^{\min} \leq \bar{u}^h \leq u^{\max}$. Furthermore, $x^{\min} \leq x \leq \alpha x = \bar{x} \leq x^{\max}$, where the last inequality holds by assumption. Thus, we conclude that $(\bar{x}, \bar{u}, \overline{\Delta l}, \bar{\sigma}, \bar{q})$ is feasible for problem (4). □ □

Theorem 3.1 does not hold for the discrete MSTSO problem (7), since the feasible set of problem (7) is discrete and finite.

To illustrate the feasibility along the rays for the continuous MSTSO problem, we consider a simple 5-bar truss structure which is shown in Figure 1.

Table 1: Parameters of the 5-bar truss structure in Figure 1.

	Bars 1-4	Bar 5
ρ	2.70 g/cm^3	6.52 g/cm^3
E	69 GPa	88 GPa
$\sigma^{\min}$, $\sigma^{\max}$	$\pm$ 172 MPa	$\pm$230 MPa
$u^{\min}$, $u^{\max}$	$\pm$ 1 cm	$\pm$ 1 cm
$x^{\min}$	0.50 cm^2	0.50 cm^2
$x^{\max}$	20 cm^2	20 cm^2

The material properties and the parameters of the 5-bar truss structure are given in Table 1. The structure is subject to two force scenarios as follows:

1. 3 kN in the negative direction x-axis direction and 3 kN in the positive direction y-axis direction exerted at node 3,

2. 12 kN in the negative direction x-axis direction and 5 kN in the positive direction y-axis direction exerted at node 4.

Bars 1-4 are assumed to have the same cross-sectional areas. The cross-sectional area of bars 1-4 is denoted by x_1 and the cross-sectional area of bar 5 is denoted by x_2.

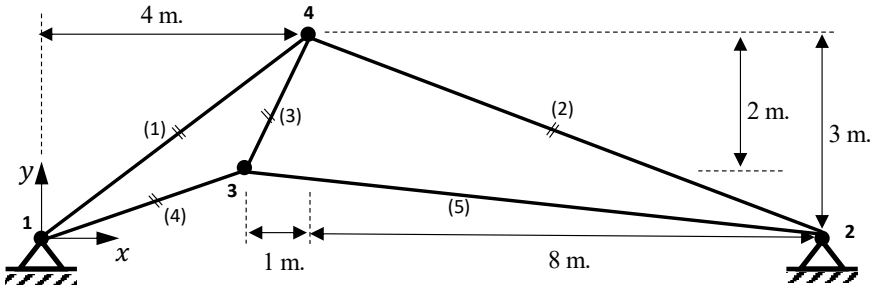

Figure 1: A 5-bar truss structure.

The feasible set projection $\mathcal{F}_{\mathcal{X}}$ of the continuous MSTSO problem (4) for the 5-bar truss is plotted in Figure 2. Figure 2, illustrates Theorem 9, that is, if x is feasible for the continuous MSTSO problem and $\alpha \geq 1$, then ray αx remains feasible as long as it does not pass the boundary defined by $x_1, x_2 \leq 20$ cm^2.

As it can be seen from Figure 2, the feasible set of the continuous MSTSO problem for the 5-bar truss is non-convex. Further, it has two local minima $x^\star = (9.75, 0.50)$ cm^2 and $\hat{x} = (5.79, 3.68)$ cm^2. The weights of the structures corresponding the $x^\star$ and $\hat{x}$ are equal to 51.34 and 52.80, respectively. Thus, $x^\star$ is the global optimal solution of the problem. We have solved the 5-bar truss problem with the solve IPOPT (Wächter and Biegler, 2006). IPOPT reports $\hat{x}$ as the solution and thus, IPOPT is not able to find the global optimal solution of the problem. The 5-bar truss demonstrates that the feasible set of a truss sizing problem can be non-convex and can have multiple local optimal solutions.

3.2 Convex hull of the external force scenarios

Convex combinations of external forces are studied in the shakedown analysis and optimal shakedown design of elsto-plastic trusses under multi-parameter static loading, (see, e.g., Giambanco and Palizzolo, 1995; Kaliszky and Lógó, 2002; Atkočiūnas et al., 2008). However, to the best of our knowledge, this concept is not studied in the optimal design of the trusses that are limited to have elastic behavior, while considering force balance equations, Hooke's law, Euler buckling constraints, yield stress, and displacement bounds.

We prove that a truss structure that withstands a set of external force scenarios also withstands a force scenario that can be written as a convex combination of the existing external force scenarios. To do so, we prove that adding a convex combination of the external force scenarios of the MSTSO problem does not change the feasible set of the problem.

Theorem 3.2. *Consider MSTSO problem (4). Let f^{p+1} be a convex combination of the external force scenarios $\{f^1, f^2, \ldots, f^p\}$, and $\tilde{\mathcal{F}}$ be the feasible set of problem (4) when external force f^{p+1} is added as a new scenario; that is, the force scenarios are given by $\{f^1, \ldots, f^p, f^{p+1}\}$ and $\tilde{\mathcal{H}} := \mathcal{H} \cup \{p+1\}$. Then, $\tilde{\mathcal{F}}_{\mathcal{X}} = \mathcal{F}_{\mathcal{X}}$.*

Proof. Clearly $\tilde{\mathcal{F}}_{\mathcal{X}} \subseteq \mathcal{F}_{\mathcal{X}}$, since $\tilde{\mathcal{H}} \supset \mathcal{H}$. Thus, we only need to prove that $\mathcal{F}_{\mathcal{X}} \subseteq \tilde{\mathcal{F}}_{\mathcal{X}}$. If $\mathcal{F} = \emptyset$, then $\tilde{\mathcal{F}} = \emptyset$, and the theorem holds. Assume that $\tilde{\mathcal{F}} \neq \emptyset$. We have assumed that $f^{p+1} = \sum_{h \in \mathcal{H}} \lambda_h f^h$, for

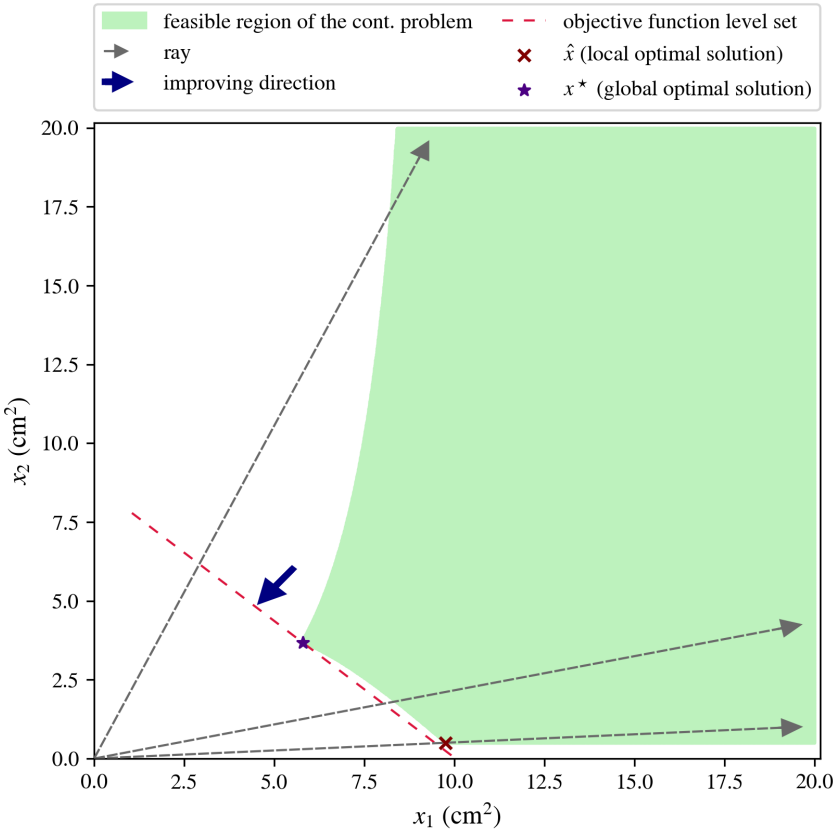

Figure 2: Feasible region of cross-sectional areas of the 5-bar truss structure.

some $\lambda_h \geq 0, h \in \mathcal{H}$ with $\sum_{h\in\mathcal{H}} \lambda_h = 1$. Let $x \in \mathcal{F}_\mathcal{X}$ be given. Then, there exists $(u, \Delta l, \sigma, q)$ such that $(x, u, \Delta l, \sigma, q) \in \mathcal{F}$. Let $(\tilde{u}, \tilde{\Delta l}, \tilde{q}, \tilde{\sigma})$ be defined by $\tilde{u} = (u, u^{p+1})$, $\tilde{\Delta l} = (\Delta l, \Delta l^{p+1})$, $\tilde{q} = (q, q^{p+1})$, and $\tilde{\sigma} = (\sigma, \sigma^{p+1})$, where

$$\begin{aligned} u^{p+1} &= \sum_{h\in\mathcal{H}} \lambda_h u^h, \\ \Delta l^{p+1} &= \sum_{h\in\mathcal{H}} \lambda_h \Delta l^h, \\ q^{p+1} &= \sum_{h\in\mathcal{H}} \lambda_h q^h, \\ \sigma^{p+1} &= \sum_{h\in\mathcal{H}} \lambda_h \sigma^h. \end{aligned} \tag{10}$$

From the fact that $(x, u, \Delta l, \sigma, q) \in \mathcal{F}$, it is enough to show that $(x, \tilde{u}, \tilde{\Delta l}, \tilde{q}, \tilde{\sigma})$ satisfies all the constraints

in (4) indexed by $h = p+1$ to conclude that $(x, \tilde{u}, \tilde{\Delta l}, \tilde{q}, \tilde{\sigma}) \in \tilde{\mathcal{F}}$. In particular note that

$$\begin{aligned} Rq^{p+1} &= R\left(\sum_{h\in\mathcal{H}} \lambda_h q^h\right) \\ &= \sum_{h\in\mathcal{H}} \lambda_h \left(Rq^h\right) \\ &= \sum_{h\in\mathcal{H}} \lambda_h f^h \\ &= f^{p+1}. \end{aligned}$$

For a given $i \in \mathcal{I}$, we know that $\sigma_i^h + \gamma_i x_i \geq 0$, for $h \in \mathcal{H}$. Multiplying each of the constraints by the corresponding λ_h and summing all the constraints, we have

$$\sum_{h\in\mathcal{H}} \lambda_h \left(\sigma_i^h + \gamma_i x_i\right) \geq 0. \tag{11}$$

From (10), we have:

$$\begin{aligned} \sum_{h\in\mathcal{H}} \lambda_h \left(\sigma_i^h + \gamma_i x_i\right) &= \sum_{h\in\mathcal{H}} \lambda_h \sigma_i^h + \left(\sum_{h\in\mathcal{H}} \lambda_h\right) \gamma_i x_i \\ &= \sigma_i^{p+1} + \gamma_i x_i. \end{aligned} \tag{12}$$

From (11) and (12), we conclude that $\sigma_i^{p+1} + \gamma_i x_i \geq 0$, for $i \in \mathcal{I}$. Similarly, all the linear constraints in (4) indexed by $h = p+1$ are satisfied. Also notice that the non-linear constraint $q_i^{p+1} - x_i \sigma_i^{p+1} = 0$, for $i \in \mathcal{I}$, holds since for a given x, the constraint becomes linear. Thus, we can conclude that $(x, \tilde{u}, \tilde{\Delta l}, \tilde{q}, \tilde{\sigma})$ satisfies all the constraints of problems (4) when the external force scenario f^{p+1} is added to the formulation. □ □

In Theorem 3.2, we prove that adding an external force scenario which is in the convex hull of the existing external force scenarios does not change the projection of the feasible set on the subspace of the cross-sectional areas. Corollary 3.3 is an extension of Theorem 3.2 where the convex hull of external force scenarios is extended towards the origin.

Corollary 3.3. *Consider the MSTSO problem (4) with the set of external forces $\{f^1, f^2, \ldots, f^p\}$. Let $\mathcal{F}_\mathcal{X}$ denote the projection of the feasible set on the subspace of the cross-sectional areas. Let $f^{p+1} = \sum_{h=1}^p \lambda_h f^h$, $\sum_{h=1}^p \lambda_h \leq 1$, and $\lambda_h \geq 0$ for $h \in \{1, \ldots, p\}$. Further, let $\tilde{\mathcal{F}}_\mathcal{X}$ denote the projection of the feasible set on the subspace of the cross-sectional areas when the force scenarios are given by $\{f^1, \ldots, f^p, f^{p+1}\}$. Then, $\tilde{\mathcal{F}}_\mathcal{X} = \mathcal{F}_\mathcal{X}$.*

Proof. Let us first add f^0 as an external force scenario to the MSTSO problem (4) and let $u^0 \in \mathbb{R}^n, \Delta l^0 \in \mathbb{R}^m, \sigma^0 \in \mathbb{R}^m$, and $q^0 \in \mathbb{R}^m$ be defined as follows:

$$u^0 = 0,\ \Delta l^0 = \sigma^0 = q^0 = 0$$

For any $x \in \mathcal{F}_\mathcal{X}$, $u^0,\ \Delta l^0,\ \sigma^0$, and q^0 satisfy all the constraints of the problem corresponding to the external force scenario f_0. Thus, adding f^0 as an external force scenario does not change the projection of the feasible set $\mathcal{F}_\mathcal{X}$.

Now consider the MSTSO problem (4) with the set of external force scenarios $\{f^0, f^1, f^2, \ldots, f^p\}$. Scenario f^{p+1} is a convex combination of the external force scenarios of this problem. This in turn reduces the corollary as a special case of Theorem 3.2. □ □

Remark 3.4. *Theorem 3.2 and Corollary 3.3 also hold for the discrete MSTSO problem (7).*

From Theorem 3.2, Corollary 3.3, and Remark 3.4, we conclude that adding an external force scenario which is in the convex hull of the existing external force scenarios extended towards the origin does not change the projection of the feasible set to the subspace of the cross-sectional areas of problems (4) and (7) and thus, nor do the optimal cross-sectional areas change. We can use this result to reduce the number of scenarios in discrete and continuous MSTSO problems by eliminating the scenarios that are redundant.

To find out whether an external force scenario $f^{\hat{h}}$ can be eliminated, one can solve the following linear feasibility problem:

$$\begin{aligned} f^{\hat{h}} &= \sum_{h \in \mathcal{H} \setminus \hat{h}} \lambda_h f^h, \\ \sum_{h \in \mathcal{H} \setminus \hat{h}} \lambda_h &\leq 1, \\ 0 \leq \lambda_h &\leq 1, \qquad h \in \mathcal{H} \setminus \hat{h}. \end{aligned} \tag{13}$$

If (13) has a solution, then the external force $f^{\hat{h}}$ can be eliminated from the set of external force scenarios without impacting the problem's optimal structure.

To identify all the external force scenarios that can be eliminated, one can start by solving the feasibility problem (13) for the external force scenario f^1 and eliminate f^1 if the corresponding feasibility problem has a solution, and iteratively do the same for all the remaining force scenarios.

To illustrate the impact of dependent scenarios on the solution time, we solved the discrete MSTSO problem for a 2D cantilever instance with 6 blocks[1] with multiple external force scenarios. The time spent on solving the problem to proven optimality is shown in Figure 3. We start by considering two linearly independent external force scenarios. Then, one-by-one, we add convex combinations of those two external force scenarios to the problem.

From Figure 3, we can see that the solution time significantly increases as the number of scenarios increases (from 2,277 seconds for the two-scenario problem to 199,089 seconds for the 12-scenario problem). Notice though that, as expected from Theorem 3.2, the optimal objective value of the problem does not change as we add external force scenarios that are convex combinations of the two original external force scenarios. On the other hand, we can apply the external-force-removal procedure that is outlined in Section 3.2. By applying the procedure, we eliminate all the dependent forces in less than 1 second. Thus, the solution time of problem (7) can be reduced up to two order of magnitude by removing scenarios that lay in the convex hull of other scenarios.

[1]The 2D cantilever truss structure is detailed in Section 4.2.4.

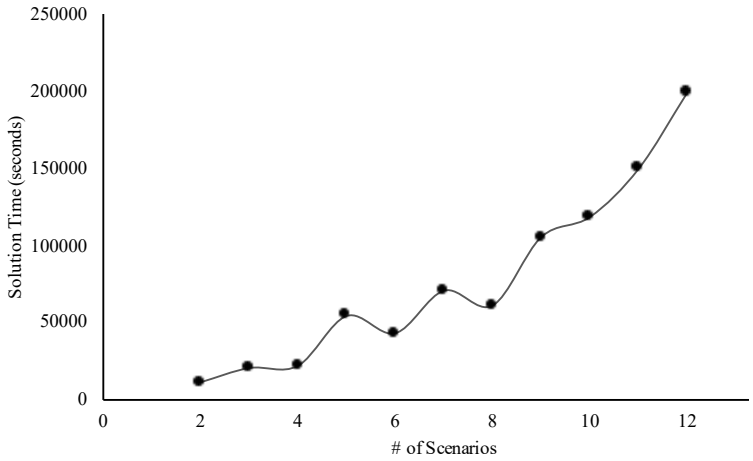

Figure 3: The effect of having dependent external forces on the solution time of the 2D cantilever with 6 blocks.

4 Computational experiments for multi-scenario TSO problems

In this section we extend the NS-MILO method developed by Shahabsafa et al. (2018), to solve large-scale MSTSO problems. Then, we demonstrate through extensive computational experiments that the extended NS-MILO method is able to solve MSTSO problems.

4.1 Extension of the NS-MILO method

The NS-MILO method is a neighborhood-search algorithm based on MILO methodologies. The NS-MILO method was proposed by Shahabsafa et al. (2018), to solve large-scale truss sizing optimization problems. In the NS-MILO method, we attempt to solve MILO subproblems iteratively. In the MILO subproblems, the size ℓ of the discrete set of each bar is at most $\ell \in \{2, 3, 5\}$.

The NS-MILO method starts by attempting to solve the continuous MSTSO problem using a non-linear optimization engine (e.g., IPOPT (Wächter and Biegler, 2006)). Then, it uses the result of Theorem 3.1 to generate an integer feasible solution through solving a sequence of MILO_2 subproblems (see Algorithm 1 for details). Having found an initial integer feasible solution, it attempts to solve a series of MILO_3 subproblems, and ultimately, a series of MILO_5 subproblems. However none of the MILO_3, nor the MILO_5 subproblems are solved to proven optimality. As soon as a better solution is found, a new MILO subproblem is defined in the neighborhood of the new integer feasible solution.

The MILO subproblems are denoted by $\text{MILO}_\ell(x)$, where the size of the discrete set of each bar is at most $\ell \in \{2, 3, 5\}$, and $x \in \mathbb{R}^m$ is a vector of cross-sectional areas of the bars. Let $\hat{\mathcal{S}}_i$ be the discrete set of bar i, for $i \in \mathcal{I}$, in subproblem $\text{MILO}_\ell(x)$. The MILO_ℓ $(\ell = 2, 3, 5)$ subproblems are defined as follows (Shahabsafa et al., 2018):

1. $\text{MILO}_2(x)$, for $x \in \mathbb{R}^m$, is the discrete MSTSO problem (7), where the discrete set of bar i, for $i \in \mathcal{I}$, is defined as
$$\hat{\mathcal{S}}_i := \begin{cases} \{s_k, s_{k+1}\}, & \text{if } s_k \leq x_i < s_{k+1}, \\ \{s_{v-1}, s_v\}, & \text{if } x_i = s_v. \end{cases}$$

2. $\text{MILO}_3(x)$, for $x_i \in \mathcal{S}$ and $i \in \mathcal{I}$, is the discrete MSTSO problem (7), where the discrete set of bar i,

for $i \in \mathcal{I}$, is defined as

$$\hat{\mathcal{S}}_i := \begin{cases} \{s_1, s_2\}, & \text{if } x_i = s_1, \\ \{s_{k-1}, s_k, s_{k+1}\}, & \text{if } x_i = s_k,\ 2 \leq k \leq v-1 \\ \{s_{v-1}, s_v\}, & \text{if } x_i = s_v. \end{cases}$$

3. MILO$_5(x)$, for $x_i \in \mathcal{S}$ and $i \in \mathcal{I}$, is the discrete MSTSO problem (7), where the discrete set of bar i, for $i \in \mathcal{I}$, is defined as

$$\hat{\mathcal{S}}_i := \begin{cases} \{s_1, s_2, s_3\}, & \text{if } x_i = s_1, \\ \{s_1, s_2, s_3, s_4\}, & \text{if } x_i = s_2, \\ \{s_{k-2}, s_{k-1}, s_k, s_{k+1}, s_{k+2}\}, & \text{if } x_i = s_k,\ 3 \leq k \leq v-2, \\ \{s_{v-3}, s_{v-2}, s_{v-1}, s_v\}, & \text{if } x_i = s_{v-1}, \\ \{s_{v-2}, s_{v-1}, s_v\}, & \text{if } x_i = s_v. \end{cases}$$

Although the NS-MILO method proposed by Shahabsafa et al. (2018) provides high-quality solutions for single-scenario TSO problems, it may fail in solving multi-scenario TSO problems. In order to extend the NS-MILO method for MSTSO problems, we make the following modifications in the NS-MILO method:

(i) Let x_c^* be the solution of the continuous MSTSO problem (4) reported by the non-linear solver. In the original NS-MILO method (Shahabsafa et al., 2018), the sequence of MILO$_2(\alpha x_c^*)$ subproblems may fail in finding an initial feasible solution for the discrete MSTSO problem. The reason for the failure is that ray αx_c^*, for $\alpha \geq 1$, may be too close to the boundary of the feasible set which in turn would decrease the likelihood of being able to generate an integer feasible solution in the neighborhood of ray αx_c^*, for $\alpha \geq 1$, in the MILO$_2$ subproblems.

To resolve this issue, we modify the NS-MILO method by increasing the lower bound of the cross-sectional areas $x^{\min}$ for the continuous problem (4) to stay away from the boundary of the feasible set of the continuous problem (4) and help MILO$_2$ subproblems to find an initial integer feasible solution. This seemingly small change significantly improves the performance of the NS-MILO method.

To illustrate the effect of increasing the lower bound of the cross-sectional areas, we again consider the 5-bar truss problem presented in Figure 1. Suppose the cross-sectional areas of the bars are selected from set $\mathcal{S} = \{0.5, 2, 4, 6, 8.5, 11, 13.5, 16.5, 20\}$ cm^2. Let $\hat{x}$ and $x^\star$ denote the solutions of the continuous MSTSO problem for the 5-bar truss problem when $x^{\min} = 0.5$ and $x^{\min} = 2$, respectively. The feasible set of the continuous MSTSO problem for the 5-bar truss is depicted in Figure 4. As it can be seen in the figure, ray $\alpha\hat{x}$, for $\alpha \geq 1$, stays close to the boundary of the feasible set, while ray $\alpha x^\star$, for $\alpha \geq 1$, is significantly away from the boundary of the feasible set.

Let $\tilde{P}$ denote the MSTSO problem (4), except that $x^{\min}$ is set to the closest value of the discrete set to $s_1 + 0.01(s_v - s_1)$. In the modified NS-MILO method, we start by solving problem $\tilde{P}$.

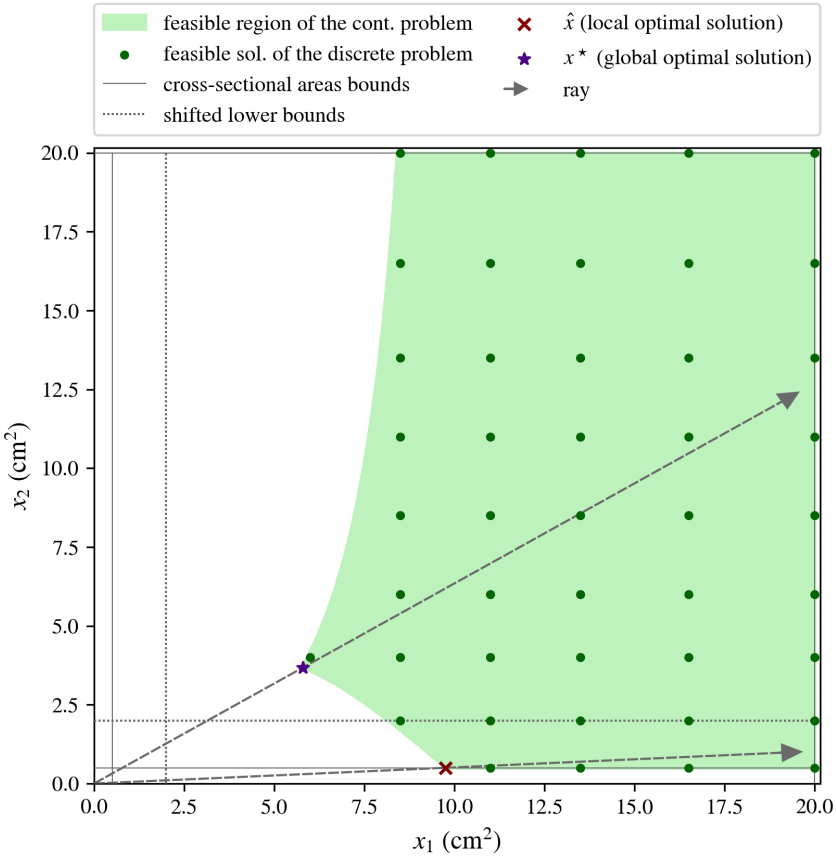

Figure 4: The effect of increasing lower bounds of cross-sectional areas of bars on the search space of the NS-MILO method.

(ii) In the original NS-MILO method (Shahabsafa et al., 2018), a constant time budget is considered in the Gurobi solver for different truss problems. To enable the NS-MILO method to solve large-scale multi-scenario TSO problems, the time budget of the MILO subproblems is set as a function of the size of the subproblems. The time budgets of the MILO$_2$ subproblems are set to be pm seconds, where p and m denote the number of scenarios and the number of bars, respectively. Additionally, the time budgets of other MILO$_\ell$ subproblems are set to be $dm\ell^2p^2$ seconds, where d is the dimension of the truss.

The outline of the NS-MILO method for MSTSO problems is presented in Algorithm 1. The subroutine "Solve($\cdot$)" returns the best solution of a problem within the time budget. The subroutine "FindSol($\cdot$)"aims to find an integer feasible solution with an objective function value better than the initially-fed integer feasible solution. The solution and the value of the objective function of the MILO subproblems are represented by $\hat{x}$ and $\hat{\eta}$, respectively.

Algorithm 1 The extended NS-MILO method for MSTSO problems

$x^0 :=$ solution of problem $\tilde{P}$
$\alpha := 1$
repeat
    $(\hat{x}, \hat{\eta}) :=$ Solve(MILO$_2(\alpha x^0)$)
    $\alpha := \alpha + 0.1$
until a feasible solution is found.
repeat
    $\eta_{\text{curr}} := \hat{\eta}$
    $(\hat{x}, \hat{\eta}) :=$ FindSol(MILO$_3(\hat{x})$)
until $\hat{\eta} = \eta_{\text{curr}}$
repeat
    $\eta_{\text{curr}} := \hat{\eta}$
    $(\hat{x}, \hat{\eta}) :=$ FindSol(MILO$_5(\hat{x})$)
until $\hat{\eta} = \eta_{\text{curr}}$
return $\hat{x}$

4.2 Computational experiments

In this section, we demonstrate how the NS-MILO method solution time scales as the size of an MSTSO problem grows. We present computational results for three classical multi-scenario test problems: the 25-bar space truss of Taye (1987), the 47-bar planar truss of Felix (1981), and the 200-bar planar truss of Thierauf and Cai (1998). Further, we consider scalable large-scale 2D and 3D cantilever and airplane wing truss structures (Shahabsafa et al., 2018). We use the IPOPT solver (Wächter and Biegler, 2006) and Gurobi 9.0.0 (2019) to solve the continuous and discrete optimization models, respectively. We compare the results of the NS-MILO method with the performance of Gurobi when directly applied to model (7). In the following, we use the acronym "Full MILO" when model (7) with the full discrete set (5) is directly solved using Gurobi. As a result, if the Full MILO approach is solved to optimality, then the solution of the Full MILO approach is a global optimal solution of the problem.

We use a desktop workstation with Dual Intel Xeon® CPU 2630 @ 2.20 GHz (20 cores) and 128 GB of RAM for all the numerical experiments. Both solvers IPOPT and Gurobi are set to use 10 threads. Since Gurobi exhausts memory in solving large-scale discrete MSTSO models, the `NodefileStart` parameter is set to 64 GB, which limits the memory usage to that amount. When the memory is at the limit, the nodes are compressed and written to a local disk. Other Gurobi parameters remain at the default values. In order to make a fair comparison between the Full MILO approach and the NS-MILO method, the time budget of the Full MILO approach is set to be equal to three times the sum of the time budgets of MILO$_3$ and MILO$_5$ subproblems, that is, $3(9 + 25)dmp^2 = 102dmp^2$.

4.2.1 The 25-bar space truss

The 25-bar space truss (Taye, 1987), shown in Figure 5, is one of the well-known multi-scenario truss structures. The density of bars' material is 0.1 lb/in^3 and the Young's modulus is 10,000 ksi. The yield stress bounds are $\pm$40,000 psi and the nodal displacements must be within $[-0.35, 0.35]$ in. The structure is subject to two force scenarios shown in Table 2. As shown in Table 2, bars in each group must have the same cross-sectional area. The cross-sectional areas of the bars are selected from set $\mathcal{S} = \{0.01, 0.4, 0.8, 1.2, 1.6, 2.0, 2.4, 2.8, 3.2, 3.6, 4.0, 4.4, 4.8, 5.2, 5.6, 6.0\}$ in^2.

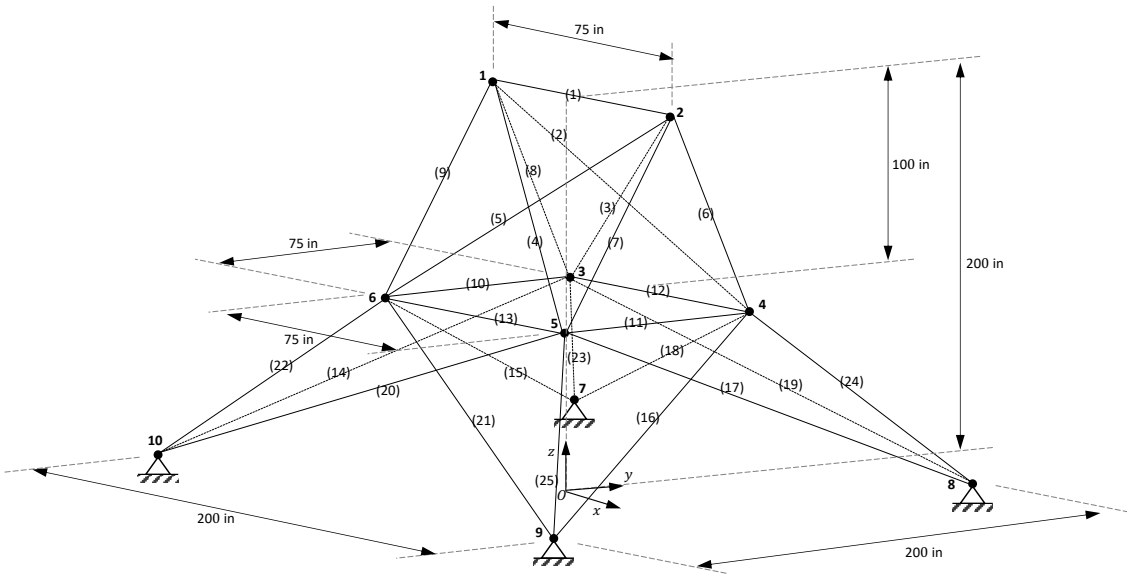

Figure 5: The 25-bar space truss structure (Taye, 1987).

Table 2: Force scenarios for the 25-bar space truss structure.

Force scenarios	Nodes	Forces (kip)		
		x-axis	y-axis	z-axis
1	1	0.0	20.0	-5.0
	2	0.0	-20.0	-5.0
2	1	0.0	10.0	-5.0
	2	1.0	10.0	-5.0
	3	0.5	0.0	0.0
	6	0.5	0.0	0.0

Table 3 shows the results obtained from the NS-MILO method and the Full MILO approach with and without considering Euler buckling constraints (3). The Full MILO approach is able to provide a global optimal solution for the 25-bar truss without and with Euler buckling constraints in 55.50 and 31.55 seconds, respectively. As shown in Table 3, the NS-MILO method also provides a global optimal solution for the 25-bar truss without and with Euler buckling constraints in 2.38 and 2.15 seconds. Thus, the NS-MILO method is more than 14 times faster than the traditional Full MILO approach for the 25-bar truss. Notice that adding Euler buckling constraints to model (7) increases the total weight of the optimal structure from 560.59 kg to 1666.26 kg. Several authors solved the discrete 25-bar space truss problem to optimality (Lee et al., 2005; Li et al., 2007; Cheng et al., 2016b).

Table 3: Optimal cross-sectional areas (in) and weights (lb) for the multi-scenario 25-bar space truss instance.

Design variables	w/o Euler buckling			w Euler buckling	
	Lee et al. (2005) Li et al. (2007) Cheng et al. (2016b)	Full MILO	NS-MILO	Full MILO	NS-MILO
x_1	0.01	0.01	0.01	0.01	0.01
$x_2 - x_5$	2.00	2.00	2.00	5.60	5.60
$x_6 - x_9$	3.60	3.60	3.60	5.60	5.60
$x_{10} - x_{11}$	0.01	0.01	0.01	0.01	0.01
$x_{12} - x_{13}$	0.01	0.01	0.01	1.60	1.60
$x_{14} - x_{17}$	0.80	0.80	0.80	4.00	4.00
$x_{18} - x_{21}$	1.60	1.60	1.60	7.20	7.20
$x_{22} - x_{25}$	2.40	2.40	2.40	5.60	5.60
Sol. time (s)	–	55.50	2.38	31.55	2.15
Weight (lb)	560.59	560.59	560.59	1666.26	1666.26

4.2.2 The 47-bar planar truss structure

Felix (1981) introduced the 47-bar planar truss structure for the shape and truss sizing optimization problem. Several meta-heuristics algorithms have been applied to the 47-bar truss for the sizing optimization problem (Lee et al., 2011; Kaveh and Mahdavi, 2014; Jalili and Hosseinzadeh, 2018). The ground structure of the 47-bar planar truss structure is illustrated in Figure 6. As shown in Table 4, the 47-bar truss structure consists of 27 groups of bars. The density of the material is 0.3 lb/in^3 and the Young's modulus is 30,000 ksi. The stress bounds of the bars are $[-15, 20]$ ksi. The truss structure should also satisfy the Euler buckling constraints where $\gamma_i = 3.96E_i/l_i^2$ for bar $i \in \{1, \ldots, 47\}$. The truss structure is subject to three force scenarios as follows:

1. 6.0 kips acting on positive x-axis direction and 14.0 kips acting on negative y-axis direction at nodes 17 and 22;
2. 6.0 kips acting on positive x-axis direction and 14.0 kips acting on negative y-axis direction at node 17;
3. 6.0 kips acting on positive x-axis direction and 14.0 kips acting on negative y-axis direction at node 22.

As shown in Table 4, bars in each group must have the same cross-sectional area. The cross-sectional areas of the bars can be selected from the discrete set $\mathcal{S} = \{0.111, 0.141, 0.196, 0.25, 0.307, 0.391, 0.442, 0.563, 0.602, 0.766, 0.785, 0.994, 1, 1.228, 1.266, 1.457, 1.563, 1.62, 1.8, 1.99, 2.13, 2.38, 2.62, 2.63, 2.88, 2.93, 3.09, 3.13, 3.38, 3.47, 3.55, 3.63, 3.84, 3.87, 3.88, 4.18, 4.22, 4.49, 4.59,4.8, 4.97, 5.12, 5.74, 7.22, 7.97, 8.53, 9.3, 10.85, 11.5, 13.5, 13.9, 14.2, 15.5, 16, 16.9, 18.8, 19.9, 22, 22.9, 24.5, 26.5, 28, 30, 33.5\}$ in^2.

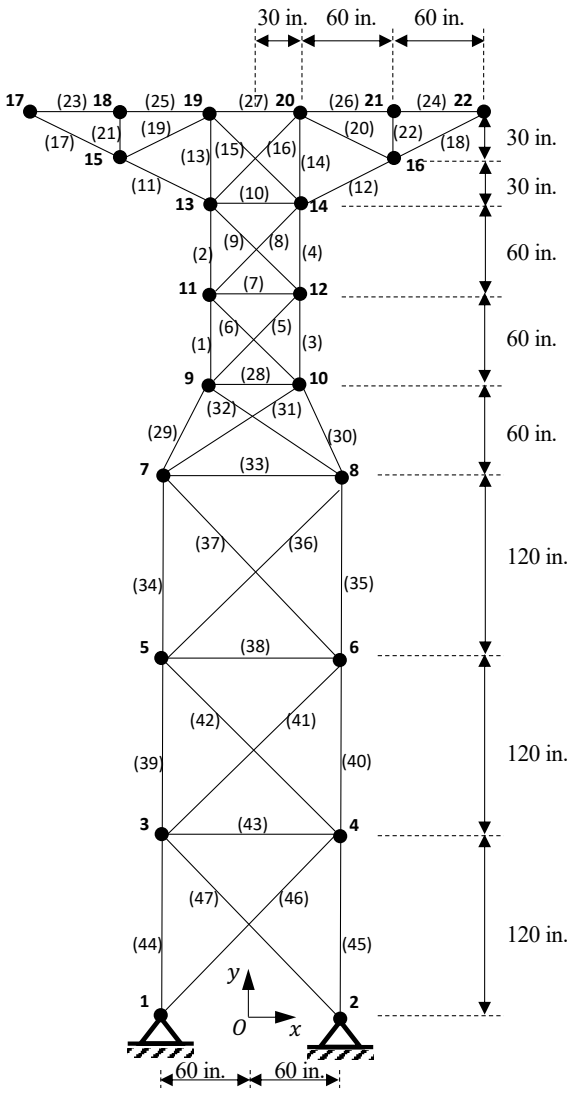

Figure 6: The 47-bar planar truss structure.

Table 4 presents the results for the 47-bar truss structure. Jalili and Hosseinzadeh (2018) found a global optimal solution after 14,400 iterations. However, they did not prove the optimality of the solution, nor did they mention how much time was spent for their algorithm to solve the problem. The Full MILO approach solves the 47-bar truss structure to proven optimality in 734 seconds, while the NS-MILO method is able to find a global optimal solution of the problem in 12 seconds (more than 60 times faster).

Table 4: The best published cross-sectional areas (in) and weights (lb) for the multi-scenario 47-bar planar truss structure.

Design variables	Lee et al. (2011)	Kaveh and Mahdavi (2014)	Jalili and Hosseinzadeh (2018)	Full MILO	NS-MILO
x_1, x_3	3.840	3.840	3.840	3.840	3.840
x_2, x_4	3.380	3.380	3.380	3.380	3.380
x_5, x_6	0.766	0.785	0.766	0.766	0.766
x_7	0.141	0.196	0.111	0.111	0.111
x_8, x_9	0.785	0.994	0.785	0.785	0.785
x_{10}	1.990	1.800	1.990	1.990	1.990
x_{11}, x_{12}	2.130	2.130	2.130	2.130	2.130
x_{13}, x_{14}	1.228	1.228	1.228	1.228	1.228
x_{15}, x_{16}	1.563	1.563	1.563	1.563	1.563
x_{17}, x_{18}	2.130	2.130	2.130	2.130	2.130
x_{19}, x_{20}	0.111	0.111	0.111	0.111	0.111
x_{21}, x_{22}	0.111	0.111	0.111	0.111	0.111
x_{23}, x_{24}	1.800	1.800	1.800	1.800	1.800
x_{25}, x_{26}	1.800	1.800	1.800	1.800	1.800
x_{27}	1.457	1.563	1.457	1.457	1.457
x_{28}	0.442	0.442	0.563	0.563	0.563
x_{29}, x_{30}	3.630	3.630	3.630	3.630	3.630
x_{31}, x_{32}	1.457	1.457	1.457	1.457	1.457
x_{33}	0.442	0.307	0.250	0.250	0.250
x_{34}, x_{35}	3.630	3.090	3.090	3.090	3.090
x_{36}, x_{37}	1.457	1.266	1.228	1.228	1.228
x_{38}	0.196	0.307	0.307	0.307	0.307
x_{39}, x_{40}	3.840	3.840	3.840	3.840	3.840
x_{41}, x_{42}	1.563	1.563	1.563	1.563	1.563
x_{43}	0.196	0.111	0.141	0.141	0.141
x_{44}, x_{45}	4.590	4.590	4.590	4.590	4.590
x_{46}, x_{47}	1.457	1.457	1.457	1.457	1.457
Weight (lb)	2,396.80	2,386.00	2,372.15	2,372.15	2,372.15

4.2.3 The 200-bar planar truss structure

The 200-bar planar truss structure is another well-known large-scale truss structure (Thierauf and Cai, 1998).

In Figure 7 the structure is illustrated. As shown in Table 5, the 200-bar planar truss structure consists of 29 groups of bars. In each group, bars must have the same cross-sectional area. The density of the material is 0.283 lb/in^3 and the Young's modulus is 30,000 ksi. The yield stress bounds of the bars are ± 10 ksi.

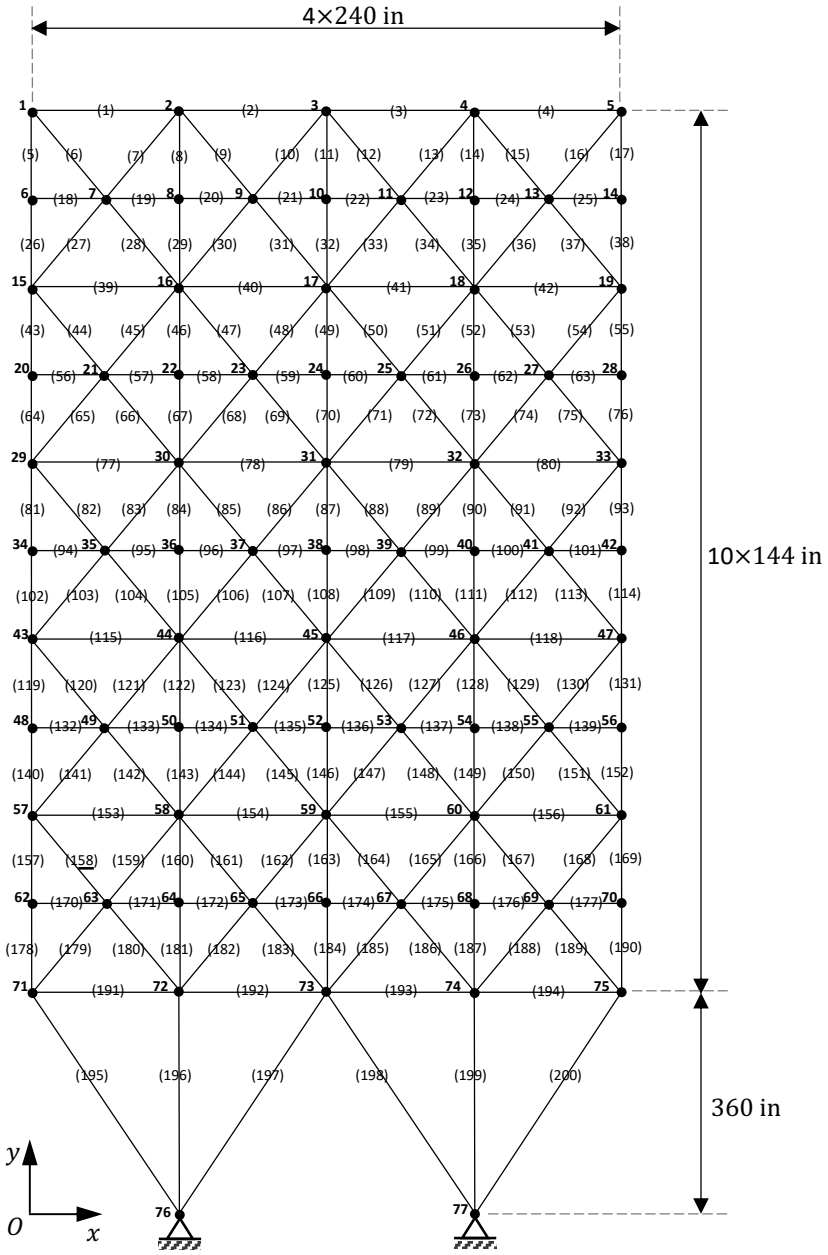

Figure 7: The 200-bar planar truss structure.

The truss structure is subject to three force scenarios as follows:

1. 1.0 kip acting in positive x-axis direction at nodes 1, 6, 15, 20, 29, 34, 43, 48, 57, 62, 71;
2. 10.0 kips acting in the negative y-axis direction at nodes 1, 2, 3, 4, 5, 6, 8, 10, 12, 14, 15, 16, 17, 18, 19, 20, 22, 24, 26, 28, 29, 30, 31, 32, 33, 34, 36, 38, 40, 42, 43, 44, 45, 46, 47, 48, 50, 52, 54, 56, 58, 59, 60, 61, 62, 64, 66, 68, 70, 71, 72, 73, 74 and 75;
3. Force scenarios 1 and 2 acting together.

The cross-sectional areas of the bars can be selected from the discrete set $\mathcal{S} = \{0.1, 0.347, 0.44, 0.539, 0.954, 1.081, 1.174, 1.333, 1.488, 1.764, 2.142, 2.697, 2.8, 3.131, 3.565, 3.813, 4.805, 5.952, 6.572, 7.192, 8.525, 9.3, 10.85, 13.33, 14.29, 17.17, 19.18, 23.68, 28.08, 33.7\}$ in^2.

Table 5: Design variables in the 200-bar planar truss problem.

Groups	Bars
$G1$	1, 2, 3, 4
$G2$	5, 8, 11, 14, 17
$G3$	19, 20, 21, 22, 23, 24
$G4$	18, 25, 56, 63, 94, 101, 132, 139, 170, 177
$G5$	26, 29, 32, 35, 38
$G6$	6, 7, 9, 10, 12, 13, 15, 16, 27, 28, 30, 31, 33, 34, 36, 37
$G7$	39, 40, 41, 42
$G8$	43, 46, 49, 52, 55
$G9$	57, 58, 59, 60, 61, 62
$G10$	64, 67, 70, 73, 76
$G11$	44, 45, 47, 48, 50, 51, 53, 54, 65, 66, 68, 69, 71, 72, 74, 75
$G12$	77, 78, 79, 80
$G13$	81, 84, 87, 90, 93
$G14$	95, 96, 97, 98, 99, 100
$G15$	102, 105, 108, 111, 114
$G16$	82, 83, 85, 86, 88, 89, 91 92, 103, 104, 106, 107, 109, 110, 112, 113
$G17$	115, 116, 117, 118
$G18$	119, 122, 125, 128, 131
$G19$	133, 134, 135, 136, 137, 138
$G20$	140, 143, 146, 149, 152
$G21$	120, 121, 123, 124, 129, 127, 129, 130, 141, 142, 144, 145, 147, 148, 150, 151
$G22$	153, 154, 155, 156
$G23$	157, 160, 163, 166, 169
$G24$	171, 172, 173, 174, 175, 176
$G25$	178, 181, 184, 187, 190
$G26$	158, 159, 161, 162, 164, 165, 167, 168, 179, 180, 182, 183, 185, 186, 188, 189
$G27$	191, 192, 193, 194
$G28$	195, 197, 198, 200
$G29$	196, 199

The results of the 200-bar truss structure are presented in Table 6. To our best knowledge, the Euler buckling constraints (3) are not considered for the 200-bar truss structure. Thus, we have compared the results of the NS-MILO method for the 200-bar truss structure without Euler buckling, with the best solutions obtained for the problem in the past. Several meta-heuristics algorithms have been applied to the 47-bar truss

for the sizing optimization problem (Azad and Hasançebi, 2014b; Hasançebi and Azad, 2015; Cheng et al., 2016b; Le et al., 2019; Degertekin et al., 2019). The best solution, found so far, for the 200-bar truss problem without Euler buckling constraints has been reported by Cheng et al. (2016b) using the HHS algorithm with the total weight of 27,163 lbs. The NS-MILO method is able to obtain a lighter solution with the total weight of 26,996 lbs for the same problem in 2,773 seconds. Notice that the Full MILO approach cannot find any solution lighter than 27,527 lbs in 367,200 seconds which is over 100 times more than the solution time of the NS-MILO method.

Further, we have compared the performance of the NS-MILO method with that of the Full MILO approach in solving the 200-bar truss problem with the Euler buckling constraints. In the 200-bar truss problem with the Euler buckling constraints, the NS-MILO method stops after 11,151 seconds with a solution of 58,288 lbs; while the Full MILO approach finds a heavier structure with a weight of 65,029 lbs in 367,200 seconds which is over 30 times more than the solution time of the NS-MILO method.

Considering the Euler buckling constraints for the 200-bar truss optimization increases the total weight of the structure and the total solution time of the NS-MILO method. The NS-MILO method solves 9 and 10 MILO subproblems in solving the 200-bar truss problem without and with considering Euler buckling constraints, respectively. Although the total number of subproblems in both cases is roughly the same, the solution time of each subproblem is an order greater than the case without Euler buckling constraints, which implies that adding the Euler buckling constraints to the 200-bar truss problem makes the problem more difficult.

As shown in Table 6, the NS-MILO method outperforms all the existing methods for the 200-bar truss structure problem without and with considering Euler buckling in terms of the total weight of the structure. Notice that the Full MILO approach is not able to solve the 200-bar truss problem without and with Euler buckling constraints to optimality in the given time budget.

4.2.4 The 2D and 3D cantilever truss structures

The 2D and the 3D cantilever trusses are scalable truss structures (Shahabsafa et al., 2018). In Figure 8, a 2D cantilever with 3 blocks is illustrated. Each block consists of 5 bars and 2 pinned nodes that are linked together. A 3D cantilever truss structures with 2 blocks is also shown in Figure 9 where each block has 20 bars and 4 pinned nodes.

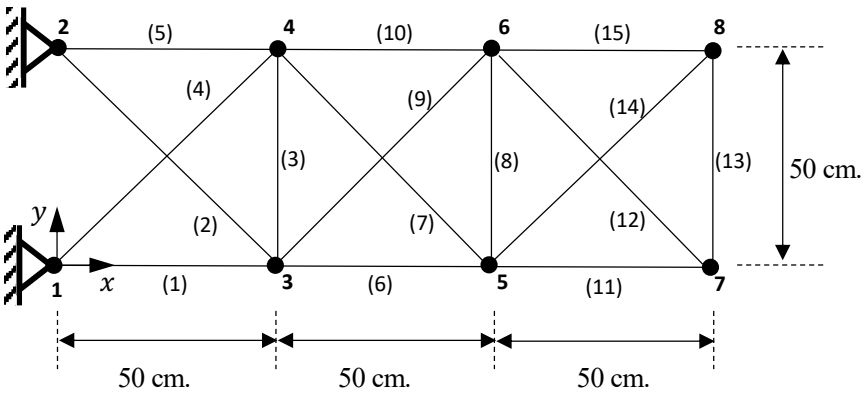

Figure 8: The 2D cantilever truss structure with three blocks.

In both the 2D and the 3D truss structures, the density of the bars' material is 2.7 g/cm^3. The Young's modulus of bars' material is 69 GPa. The yield stress bounds are ± 172.36 MPa. Let n_b denote the number

Table 6: The best published cross-sectional areas (in^2) and weights (kip) for the multi-scenario 200-bar planar truss structure.

Groups	w/o Euler buckling							w Euler buckling	
	Azad and Hasanebi (2014b)	Hasanebi and Azad (2015)	Cheng et al. (2016b)	Le et al. (2019)	Degertekin et al. (2019)	Full MILO	NS-MILO	Full MILO	NS-MILO
$G1$	0.100	0.100	0.100	0.100	0.100	0.347	0.347	1.488	1.488
$G2$	0.954	0.954	0.954	0.954	0.954	0.954	0.954	2.697	2.800
$G3$	0.100	0.347	0.100	0.347	0.347	0.100	0.100	0.347	0.440
$G4$	0.100	0.100	0.100	0.100	0.100	0.100	0.100	0.954	0.954
$G5$	2.142	2.142	2.142	2.142	2.142	2.142	2.142	4.805	4.805
$G6$	0.347	0.347	0.347	0.347	0.347	0.347	0.347	2.697	2.800
$G7$	0.100	0.100	0.100	0.100	0.100	0.100	0.100	3.565	1.333
$G8$	3.131	3.131	3.131	3.131	3.131	3.131	3.565	5.952	4.805
$G9$	0.100	0.100	0.100	0.100	0.100	0.100	0.100	2.697	0.440
$G10$	4.805	4.805	4.805	4.805	4.805	4.805	4.805	6.572	5.952
$G11$	0.347	0.440	0.440	0.440	0.440	0.347	0.440	4.805	3.813
$G12$	0.100	0.100	0.347	0.347	0.347	0.100	0.100	1.764	1.174
$G13$	5.952	5.952	5.952	5.952	5.952	5.952	5.952	6.572	6.572
$G14$	0.100	0.100	0.347	0.347	0.100	0.100	0.100	0.347	0.440
$G15$	6.572	6.572	6.572	6.572	6.572	6.572	6.572	9.300	7.192
$G16$	0.440	0.539	0.954	0.954	0.954	0.440	0.539	4.805	4.805
$G17$	0.539	0.100	0.347	0.347	0.100	0.100	0.347	1.174	1.488
$G18$	7.192	8.525	8.525	8.525	8.525	8.525	8.525	9.300	9.300
$G19$	0.440	0.539	0.100	0.100	0.539	0.100	0.347	3.131	0.440
$G20$	8.525	9.300	9.300	9.300	9.300	8.525	9.300	13.330	9.300
$G21$	0.954	0.954	1.081	0.954	0.954	0.539	0.954	5.952	4.805
$G22$	1.174	0.100	0.347	1.333	0.100	1.174	0.100	2.142	2.142
$G23$	10.850	10.850	13.330	13.330	13.330	10.850	13.330	9.300	9.300
$G24$	0.440	0.954	0.954	0.347	0.100	0.539	0.100	2.697	0.539
$G25$	10.850	13.330	13.330	13.330	13.330	10.850	13.330	10.850	10.850
$G26$	1.764	1.333	1.764	2.142	0.954	1.333	0.954	8.525	5.952
$G27$	8.525	7.192	3.813	3.813	5.952	8.525	5.952	3.131	9.300
$G28$	13.330	10.850	8.525	8.525	10.850	13.330	10.850	28.080	28.080
$G29$	13.330	14.290	17.170	17.170	14.290	13.330	14.290	33.700	28.080
Weight (kips)	28.075	27.190	27.163	27.421	27.282	27.527	26.996	65.029	58.288

of blocks. The displacements of nodes must be between $\pm 0.1 n_b^2$ cm. In both the 2D and the 3D cantilever truss structures, the cross-sectional areas of the bars can be selected from set $\mathcal{S} = \{0.25, 0.5, 0.75, 1, 2, 3, 4, 6, 7, 8, 9, 10, 12, 14, 16, 18, 20, 22, 24, 26, 28, 30, 32, 34, 36, 38, 40, 42.5, 45, 47.5, 50, 52.5, 55, 57.5, 60, 62.5, 65, 70, 75, 80, 85\}$ cm^2.

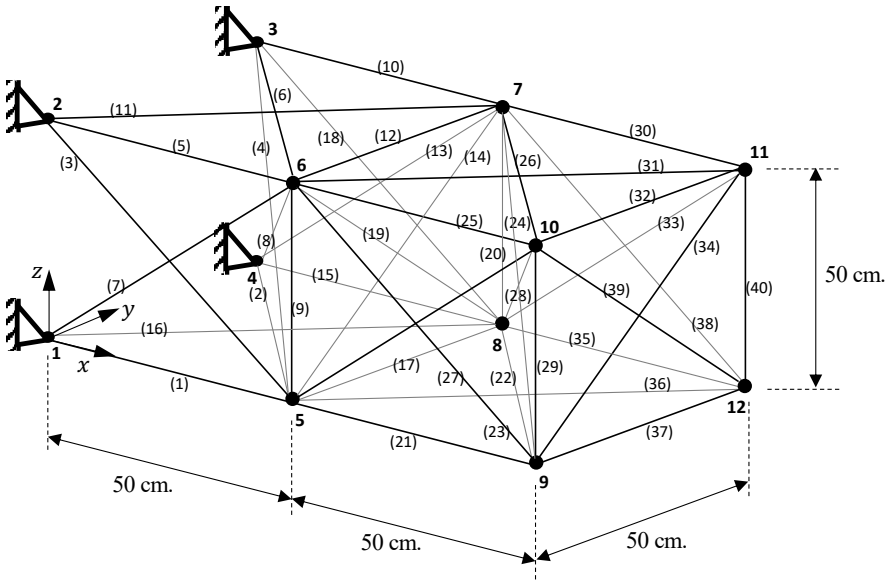

Figure 9: The 3D cantilever truss structure with two blocks.

The 2D and 3D cantilever truss structures are subject to two and three force scenarios, respectively. The external force scenarios for all the 2D and 3D cantilever are provided in the supplementary material[2].

Table 7: Structure weights (kg) and solution times (seconds) for the best solutions found by the Full MILO and the NS-MILO methods for the two-scenario 2D cantilever truss structures.

n_b	m	Full MILO			NS-MILO			w_f/w_n
		opt. gap(%)	w_f	t_f	n_s	w_n	t_n	
4	20	0.00	10.31	189	9	10.31	5	1.00
12	60	11.98	37.18	48,960	11	37.15	2,690	1.00
24	120	14.25	88.82	97,920	19	88.06	22,916	1.01
36	180	16.85	193.83	146,880	31	190.64	12,472	1.02
48	240	16.82	342.25	195,840	30	339.20	79,549	1.01
60	300	15.85	474.01	244,800	30	471.32	73,444	1.01

The results of the Full MILO approach and the NS-MILO method for two-scenario 2D cantilever truss structures are presented in Table 7. It should be noted in that Table 7 “opt. gap" is the ratio of the difference of the best upper and lower bounds of the objective function found by Gurobi divided by the upper bound. In all the cases, the NS-MILO found a solution at least as good as the Full MILO in a smaller time. As the size of the problems grow, the number of the subproblems in the NS-MILO method and the optimality gap in the Full MILO approach increases.

The results of the Full MILO approach and the NS-MILO method for three-scenario 3D cantilever truss structures are presented in Table 8. In all the cases, the NS-MILO method outperforms the Full MILO approach with respect to the solution quality and solution time. In large 3D cantilever problems, the solution quality of the Full MILO drops to a great extent; while the NS-MILO method still provides high-quality solutions in a reasonable amount of time. In the largest instance, the weight of the solution obtained from the Full-MILO method is more than three times of that of the solution obtained from the NS-MILO approach. Notice in the Full MILO approach that the optimality gap increases rapidly as the size of problem grows.

We observe that in Tables 7 and 8 the solution time of the NS-MILO method for the 3D cantilever structures is significantly more than that of the NS-MILO method for the 2D cantilever structures with the

[2]https://github.com/shahabsafa/truss-data.git

Table 8: Structure weights (kg) and solution times (seconds) for the best solutions found by the Full MILO and the NS-MILO methods for the three-scenario 3D cantilever truss structures.

n_b	m	Full MILO			NS-MILO			w_f/w_n
		opt. gap(%)	w_f	t_f	n_s	w_n	t_n	
1	20	20.88	14.41	55,080	15	14.26	1,337	1.01
3	60	51.11	38.99	165,240	14	37.62	75,653	1.04
6	120	67.39	126.85	330,480	27	88.02	202,672	1.44
9	180	68.68	252.91	495,720	32	154.73	541,089	1.63
12	240	70.27	408.67	660,960	20	222.77	311,163	1.83
15	300	82.69	1,019.56	826,200	30	315.98	999,078	3.23

same number of bars. This indicates that the 3D cantilever problems are significantly harder than the 2D cantilever problems. Further, we observe that the ratio w_f/w_n increases from 2D cantilever to 3D cantilever trusses with the same number of bars. This indicates that the Full-MILO approach is adversely affected as the structures get more sophisticated while the NS-MILO method is still able to provide high-quality solutions for those sophisticated structures.

4.2.5 Wing truss structures

The airplane wing trusses are 3D truss structures (Shahabsafa et al., 2018). We consider the wing truss structures subject to three force scenarios. In all the wing trusses, the Young's modulus of the bars' material is 69 GPa and the density of the bars' material is 2.7 g/cm^3. The yield stress is equal to ± 270 MPa. It is assumed that there are no bounds on the nodal displacements of the structure. The force scenarios along with the data of the nodes and bars of the wing structures are provided as a supplementary material[3]. The cross-sectional areas of the bars can be selected from set $\mathcal{S} = \{0.25, 1, 5, 10, 15, 20, 25, 30, 35, 40, 45, 50, 55, 60, 65, 70, 75, 80, 85, 90, 95, 100, 150, 200, 250, 300, 350, 400, 450, 500, 550, 600, 650, 700, 750, 800, 850, 900, 950, 1000, 1050, 1100, 1150, 1200\}$ cm^2.

There are three load scenarios considered in this test corresponding to three different aircraft weights: 95%, 84%, and 61% of maximum take-off weight (MTOW). The distribution of the loads is determined by AVL, an aerodynamic panel code (Drela and Youngren, 2010). The loads are transferred to the truss structure from the aerodynamic mesh by associating every aerodynamic mesh node to the closest truss node. In the process, the forces are directly passed to the truss node.

In Table 9, the results of the Full MILO approach and the NS-MILO method for the three-scenario wing truss structures are provided. As the size of the wing trusses grow, the optimality gap of the Full MILO approach increases, implying that the Full MILO approach essentially fails in providing high-quality solutions for large-scale wing trusses. However, the relative solution quality of the NS-MILO method and the Full MILO approach (w_f/w_n) increases as the size of the wing trusses grow demonstrating that the NS-MILO method is able to obtain significantly lighter structures for all the wing trusses. For example, the weight of the 315-bar wing truss obtained by the Full MILO approach is 5.69 times more than that of the solution obtained by the NS-MILO method.

It can be seen in Table 9 that the number of explored branch and bound (B&B) nodes in the NS-MILO method is greater than that of the Full MILO approach. It is because of the fact that the size of MILO subproblems of the NS-MILO method is smaller than the original MILO problem (7) considered in the Full MILO approach. However, due to the curse of dimensionality, the number of solved subproblems in the NS-MILO method decreases as the size of problems increase.

In the Full-MILO approach, for the 279-bar and 315-bar wing trusses, Gurobi stops with `segmentation`

[3] https://github.com/shahabsafa/truss-data.git

`fault` error before reaching the specified time limit. Notice in Table 9 that the specified time budget of the Full MILO approach for all the wing trusses is greater than the solution time of the NS-MILO method except for the 207-bar wing truss.

Table 9: Structure weights (kg) and solution times (seconds) for the best solutions found by the Full MILO and the NS-MILO methods for the three-scenario 3D wing truss structures.

m	Full MILO				NS-MILO				w_f/w_n
	opt. gap(%)	B&B nodes	w_f	t_f	n_s	B&B nodes	w_n	t_n	
81	50.56	137,456	23,622.96	223,074	84	31,080,713	18,969.21	82,987	1.25
117	68.34	45,881	24,639.76	322,218	93	3,869,281	14,226.04	179,298	1.73
153	77.59	24,012	28,633.69	421,362	77	12,024,500	12,080.19	406,253	2.37
207	86.98	11,971	45,849.12	570,078	46	3,481,214	10,589.57	723,501	4.33
243	91.85	9,211	72,642.14	669,222	63	1,401,785	9,667.33	463,967	7.51
279	92.70	632	79,323.30	287,691	38	857,267	10,324.33	472,967	7.68
315	90.00	306	58,052.70	305,212	18	310,347	10,193.65	359,339	5.69

The solution of the 315-bar case is shown in Figure 10. The first load scenario has most bars with active stress and buckling constraints. The second and third scenarios have several bars with active buckling constraints as well. This is expected because the first load scenario has the largest lift. The second and third load also affect the optimization results because the load distributions are linearly independent. Thus, Theorem 3.2 and Corollary 3.3 are not applicable here.

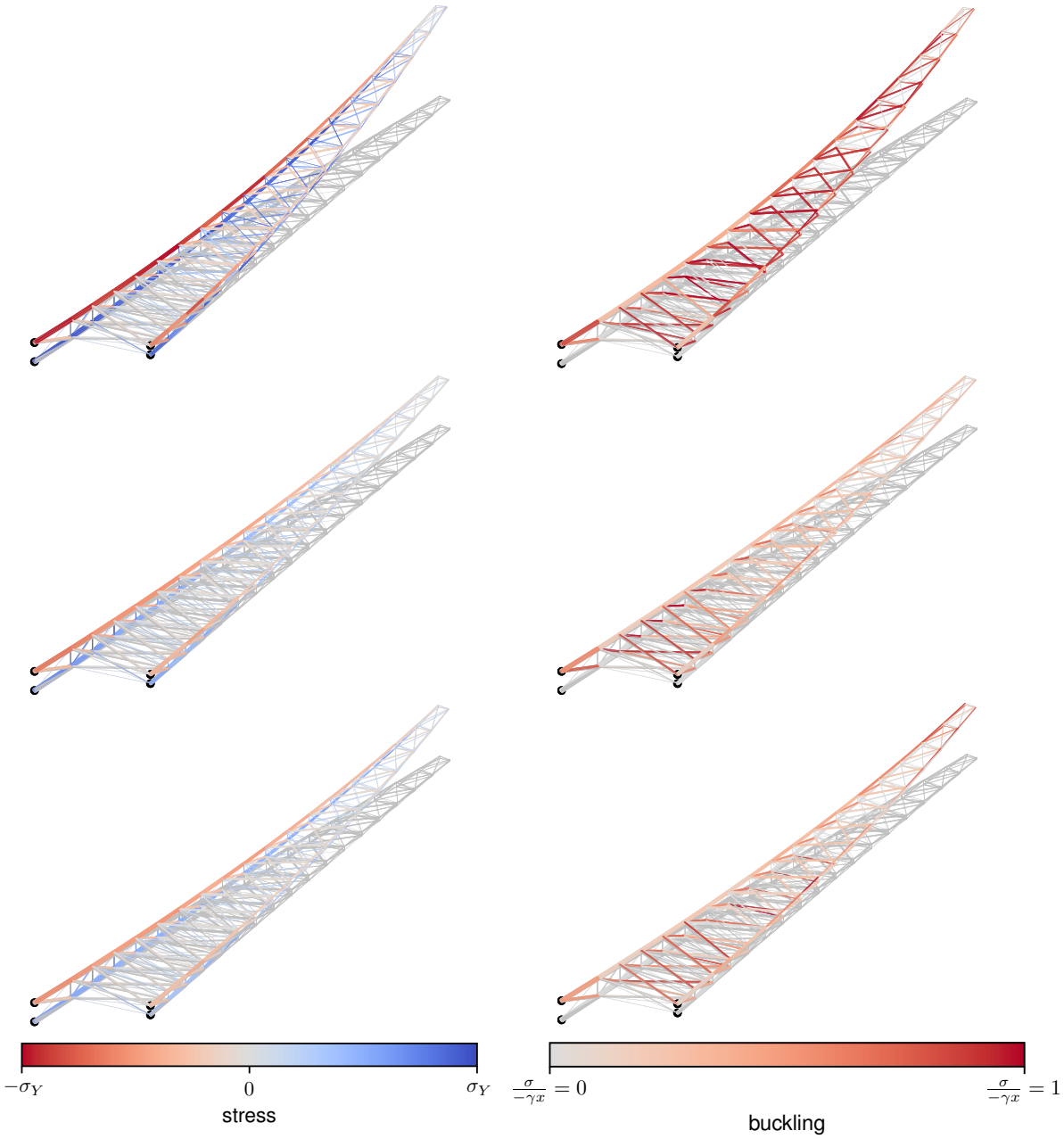

Figure 10: Optimized wing with 315 bars stress and buckling failure parameter distribution under three different load scenarios, where the undeformed truss is shown in light gray. The buckling failure parameter is set to zero for the bars in tension.

5 Conclusions and future research

In this paper, we presented two important characteristics of multi-scenario truss sizing optimization (MSTSO) problems. We proved that for a given feasible solution of the continuous MSTSO problem, an appropriate scaling of cross-sectional areas of the truss structure preserves the feasibility of the new structure for the same problem. This property is used in the neighborhood search mixed integer linear optimization (NS-MILO) method. Second, we proved that adding a convex combination of external force scenarios does not change the feasible set of the MSTSO problem. Thus, we can utilize this characteristic to eliminate redundant force

scenarios to reduce the solution time.

We also extended the NS-MILO method to solving large-scale multi-scenario truss sizing optimization problems. We applied the extended NS-MILO method to solve different classical and large-scale MSTSO test problems. The computational experiments confirmed the high performance of the extended NS-MILO method for solving discrete MSTSO problems. Further work can be done to develop the NS-MILO method for solving large-scale discrete multi-scenario truss topology design and sizing optimization problems.

Acknowledgment

This research was supported by Air Force Office of Scientific Research Grant #FA9550-15-1-0222.

References

Achtziger, W. (1998). Multiple-load truss topology and sizing optimization: Some properties of minimax compliance. *Journal of Optimization Theory and Applications*, 98(2):255–280.

Achtziger, W. and Stolpe, M. (2007a). Global optimization of truss topology with discrete bar areas—part I: theory of relaxed problems. *Computational Optimization and Applications*, 40(2):247–280.

Achtziger, W. and Stolpe, M. (2007b). Global optimization of truss topology with discrete bar areas—part II: Implementation and numerical results. *Computational Optimization and Applications*, 44(2):315–341.

Achtziger, W. and Stolpe, M. (2007c). Truss topology optimization with discrete design variables—guaranteed global optimality and benchmark examples. *Structural and Multidisciplinary Optimization*, 34(1):1–20.

Alvarez, F. and Carrasco, M. (2005). Minimization of the expected compliance as an alternative approach to multiload truss optimization. *Structural and Multidisciplinary Optimization*, 29(6):470–476.

Atkočiūnas, J., Merkevičiūtė, D., and Venskus, A. (2008). Optimal shakedown design of bar systems: Strength, stiffness and stability constraints. *Computers & Structures*, 86(17):1757–1768.

Azad, S. K. and Hasançebi, O. (2015). Discrete sizing optimization of steel trusses under multiple displacement constraints and load cases using guided stochastic search technique. *Structural and Multidisciplinary Optimization*, 52(2):383–404.

Azad, S. K. and Hasançebi, O. (2014a). An elitist self-adaptive step-size search for structural design optimization. *Applied Soft Computing*, 19:226 – 235.

Azad, S. K. and Hasançebi, O. (2014b). An elitist self-adaptive step-size search for structural design optimization. *Applied Soft Computing*, 19:226 – 235.

Ben-Tal, A. and Bendsøe, M. P. (1993). A new method for optimal truss topology design. *SIAM Journal on Optimization*, 3(2):322–358.

Ben-Tal, A. and Nemirovski, A. (2001). *Lectures on modern convex optimization: analysis, algorithms, and engineering applications*. SIAM.

Calafiore, G. C. and Dabbene, F. (2008). Optimization under uncertainty with applications to design of truss structures. *Structural and Multidisciplinary Optimization*, 35(3):189–200.

Camp, C. and Farshchin, M. (2014). Design of space trusses using modified teaching–learning based optimization. *Engineering Structures*, 62-63:87 – 97.

Capriles, P. V. S. Z., Fonseca, L. G., Barbosa, H. J. C., and Lemonge, A. C. C. (2007). Rank-based ant colony algorithms for truss weight minimization with discrete variables. *Communications in Numerical Methods in Engineering*, 23(6):553–575.

Cheng, M.-Y., Prayogo, D., Wu, Y.-W., and Lukito, M. M. (2016a). A hybrid harmony search algorithm for discrete sizing optimization of truss structure. *Automation in Construction*, 69:21 – 33.

Cheng, M.-Y., Prayogo, D., Wu, Y.-W., and Lukito, M. M. (2016b). A hybrid harmony search algorithm for discrete sizing optimization of truss structure. *Automation in Construction*, 69:21 – 33.

Csébfalvi, A. (2018). Structural optimization under uncertainty in loading directions: Benchmark results. *Advances in Engineering Software*, 120:68 – 78. Civil-Comp - Part 2.

Degertekin, S. (2012). Improved harmony search algorithms for sizing optimization of truss structures. *Computers & Structures*, 92-93:229 – 241.

Degertekin, S., Lamberti, L., and Ugur, I. (2019). Discrete sizing/layout/topology optimization of truss structures with an advanced jaya algorithm. *Applied Soft Computing*, 79:363 – 390.

Do, D. T. and Lee, J. (2017). A modified symbiotic organisms search (msos) algorithm for optimization of pin-jointed structures. *Applied Soft Computing*, 61:683 – 699.

Dorn, W. S., Gomory, R. E., and Greenberg, H. J. (1964). Automatic design of optimal structures. *Journal de Mecanique*, 3:25–52.

Drela, M. and Youngren, H. (2010). *AVL 3.30 User Primer*. MIT.

Dunning, P. D., Kim, H. A., and Mullineux, G. (2011). Introducing loading uncertainty in topology optimization. *AIAA Journal*, 49(4):760–768.

Felix, J. E. (1981). Shape optimization of trusses subject to strength, displacement, and frequency constraints. Master's thesis, Mechanical Engineering Department, Naval Postgraduate School, USA.

Giambanco, F. and Palizzolo, L. (1995). Optimality conditions for shakedown design of trusses. *Computational Mechanics*, 16(6):369–378.

Gurobi Optimization Inc. (2019). Gurobi optimizer reference manual.

Hasançebi, O. and Azad, S. K. (2015). Adaptive dimensional search: A new metaheuristic algorithm for discrete truss sizing optimization. *Computers & Structures*, 154:1 – 16.

Jalili, S. and Hosseinzadeh, Y. (2018). Design optimization of truss structures with continuous and discrete variables by hybrid of biogeography-based optimization and differential evolution methods. *The Structural Design of Tall and Special Buildings*, 27(14):e1495. e1495 TAL-17-0234.R2.

Kaliszky, S. and Lógó, J. (2002). Plastic behaviour and stability constraints in the shakedown analysis and optimal design of trusses. *Structural and Multidisciplinary Optimization*, 24(2):118–124.

Kanno, Y. and Takewaki, I. (2006). Sequential semidefinite program for maximum robustness design of structures under load uncertainty. *Journal of Optimization Theory and Applications*, 130(2):265.

Kaveh, A. and Mahdavi, V. (2014). Colliding bodies optimization method for optimum discrete design of truss structures. *Computers & Structures*, 139:43 – 53.

Lamberti, L. (2008). An efficient simulated annealing algorithm for design optimization of truss structures. *Computers & Structures*, 86(19):1936 – 1953.

Le, D. T., Bui, D.-K., Ngo, T. D., Nguyen, Q.-H., and Nguyen-Xuan, H. (2019). A novel hybrid method combining electromagnetism-like mechanism and firefly algorithms for constrained design optimization of discrete truss structures. *Computers & Structures*, 212:20 – 42.

Lee, K., Han, S., and Geem, Z. a. (2011). Discrete size and discrete-continuous configuration optimization methods for truss structures using the harmony search algorithm. *International Journal of Optimization in Civil Engineering*, 1:107–126.

Lee, K. S., Geem, Z. W., ho Lee, S., and woong Bae, K. (2005). The harmony search heuristic algorithm for discrete structural optimization. *Engineering Optimization*, 37(7):663–684.

Li, L., Huang, Z., Liu, F., and Wu, Q. (2007). A heuristic particle swarm optimizer for optimization of pin connected structures. *Computers & Structures*, 85(7):340 – 349.

Liu, J. and Gea, H. C. (2018). Robust topology optimization under multiple independent unknown-but-bounded loads. *Computer Methods in Applied Mechanics and Engineering*, 329:464–479.

Lógó, J., Ghaemi, M., and Rad, M. M. (2009). Optimal topologies in case of probabilistic loading: The influence of load correlation. *Mechanics Based Design of Structures and Machines*, 37(3):327–348.

Makrodimopoulos, A., Bhaskar, A., and Keane, A. J. (2010). A compliance based design problem of structures under multiple load cases. *Structural and Multidisciplinary Optimization*, 42(5):739–743.

Mela, K. (2014). Resolving issues with member buckling in truss topology optimization using a mixed variable approach. *Structural and Multidisciplinary Optimization*, 50(6):1037–1049.

Mellaert, R. V., Lombaert, G., and Schevenels, M. (2016). Global size optimization of statically determinate trusses considering displacement, member, and joint constraints. *Journal of Structural Engineering*, 142(2):04015120.

Pedersen, P. (1993). *Topology Optimization of Three-Dimensional Trusses*, pages 19–30. Springer Netherlands, Dordrecht.

Shahabsafa, M., Mohammad-Nezhad, A., Terlaky, T., Zuluaga, L., He, S., Hwang, J. T., and Martins, J. R. (2018). A novel approach to discrete truss design problems using mixed integer neighborhood search. *Structural and Multidisciplinary Optimization*, 58(6):2411–2429.

Smith, O. (1997). Topology optimization of trusses with local stability constraints and multiple loading conditions—a heuristic approach. *Structural Optimization*, 13(2):155–166.

Stolpe, M. (2004). Global optimization of minimum weight truss topology problems with stress, displacement, and local buckling constraints using branch-and-bound. *International Journal for Numerical Methods in Engineering*, 61(8):1270–1309.

Stolpe, M. (2016). Truss optimization with discrete design variables: a critical review. *Structural and Multidisciplinary Optimization*, 53(2):349–374.

Taye, S. (1987). *Approximation concepts in optimum structural design*. PhD thesis, Technion-Israel Institute of technology, Faculty of civil engineering, Israel.

Thierauf, G. and Cai, J. (1998). Parallelization of the evolution strategy for discrete structural optimization problems. *Computer-Aided Civil and Infrastructure Engineering*, 13(1):23–30.

Topping, B. H. V. (1983). Shape optimization of skeletal structures: A review. *Journal of Structural Engineering*, 109(8):1933–1951.

Wächter, A. and Biegler, L. T. (2006). On the implementation of an interior-point filter line-search algorithm for large-scale nonlinear programming. *Mathematical Programming*, 106(1):25–57.

Zhao, J. and Wang, C. (2014). Robust topology optimization under loading uncertainty based on linear elastic theory and orthogonal diagonalization of symmetric matrices. *Computer Methods in Applied Mechanics and Engineering*, 273:204–218.